Robotica (2023), **41**, pp. 1634–1650
doi:10.1017/S026357472300005X

CAMBRIDGE UNIVERSITY PRESS

RESEARCH ARTICLE

Design of motor cable artificial muscle (MC-AM) with tendon sheath–pulley system (TSPS) for musculoskeletal robot

Jianbo Yuan*, Yerui Fan and Yaxiong Wu

School of Mechanical Engineering, University of Science and Technology Beijing, Beijing 100083, China
*Corresponding author. E-mail: jianbo.yuan@qq.com.

Received: 27 September 2022; **Revised:** 20 November 2022; **Accepted:** 28 December 2022;
First published online: 10 February 2023

Keywords: motor cable artificial muscle, tendon sheath–pulley system, feed-forward multi-layer neural network, friction compensation, lightweight musculoskeletal arm

Abstract

In an unstructured environment, the arm can perform complicated tasks with rapidity, flexibility, and robustness. It is difficult to configure multiple artificial muscles similar to an arm in the compact space of a robotic arm. When muscle tension is transferred, mechanisms like tendon-sheath/tendon-pulley may be installed in a compact space to develop musculoskeletal robots that are closer to the arm. However, handling variable frictional nonlinearity and elastic cable deformation is necessary for transmission stability. In this study, the modular artificial muscle system (MAMS), including motor cable artificial muscle and tendon sheath–pulley system (TSPS), that can be installed remotely and transmit muscle tension in narrow paths, is designed. The feed-forward multi-layer neural network (FF-MNN) approach is utilized to discuss the relationship between the measurable input tension of TSPS and the unmeasurable output tension and cable elongation. Subsequently, the lightweight musculoskeletal arm (LM-Arm) is built to verify the validity of MAMS. Through trials, the experiments of MAMS after friction compensating and the LM-Arm's end-point 3D trajectory tracking are investigated. The results show that average errors of the active and passive muscles tension are 3.87 N and 3.51 N, respectively, under conditions of larger load and higher contraction velocity. The average muscle length error of trajectory tracking is 0.00078 m (0.72%). The suggested MAMS may successfully build a musculoskeletal robot that has similar flexibility and morphology to the arm. It can also be utilized to power various pieces of machinery, such as rescue robot, invasive surgical robots, dexterous hands, and wearable exoskeletons.

1. Introduction

Redundantly configured muscles and flexible skeletal structures can be found in human arm [1]. It can rapidly, flexibily, and robustly execute difficult operation tasks. Muscles are composed of tendons and fibers, whose unique physical structure and control mechanism of neural signal excitation enable them to demonstrate strong compliance and robustness [2–5]. Designing an artificial muscle that can replace muscle to drive a musculoskeletal robot is difficult. There are several demands of the artificial muscle system for the musculoskeletal robot: (1) Multiple artificial muscles should be installed in a small space to power skeletal movement; (2) The artificial muscle should be capable of rapid contraction/relaxation with large load and shrinkage ratio to satisfy the rapid and flexible movement of skeleton; (3) Two working states of active and passive artificial muscle should be imitated to satisfy antagonistic relationship between multiple muscles. To explore devices that can replace muscles, several artificial muscles have been investigated [6–10]. Pneumatic artificial muscle (PAM) and MC-AM are currently the two most popular driving techniques [11, 12]. There are others technology that cannot be matured, such as fiber-based artificial muscle [13], twisted and coiled soft actuators [9], and novel material artificial muscle

[10]. According to the PAM theory, the cavity naturally resembles muscle in physical tissues in that it contracts or expands in response to variations in internal air/hydraulic pressure. However, it is challenging to operate the robot steadily and safely due to the issues, including gas/oil leaking, tough control, and complex attachments. The MC-AM, which offers several benefits, including mature control technology, high energy density, convenient installation, and removable power, is becoming the top option for artificial muscle power.

In the previous work [14], the MC-AM was designed, but insufficient consideration was given to the way of muscle tension transmission. Conforming to particular work situations that necessitate a difficult transmission path (limited space and varied shape), the TSPS frequently collaborates with MC-AM to power remote devices without adding unnecessary components to them. It is frequently used in applications with limited installation space, such as humanoid robotic hands [15], exoskeleton [16], parallel robots [17], and invasive surgical robot [18]. But the TSPS also has problems such as nonlinear friction, time-varying hysteresis, and elastic deformation of the cable. To address this issue, output feedback control techniques are frequently employed [19, 20]. The arm's forearm, wrist, fingers, and other areas have an exceptionally high concentration of muscles, making it difficult to implant tension sensors. In the conditions of remote sensorless, Wang *et al.* [21] focused on the friction analysis for the fixed-path tendon sheath configurations, and the effect of tendon length on friction attenuation was modeled. Subsequently, Sun *et al.* [22] proposed a remedy to enhance the system tolerance against potential unmodeled perturbations along the transmission route during operation. Do *et al.* [23] combined the Stribeck function and the modified normalized Bouc-Wen model to model the tendon sheath friction characteristics when discontinuity as the system operates near areas of zero velocity. Wu *et al.* [24] proposed a general mathematical double tendon sheath transmission model suitable for arbitrary types of load conditions and executed the torque/position-tracking experiments. Wang *et al.* [25] established an analytic and compact model for cable guiding mechanisms, and the velocity and acceleration mapping from the moving platform to the cables was derived. Jeong *et al.* [26] proposed a novel method of compensating for the changing nonlinearity of the Bowden cable based on a Bowden-cable angle sensor. The above researchers have studied friction compensation for a range of tendon sleeve/tendon pulley applications and obtained satisfactory results. However, there are still some shortcomings, such as the need for the feedback of sheath bending angle, small load capacity, and single application scenario.

In real-world applications, the TSPS can have a variety of unpredictable impacts, including variations in lubricant viscosity, manufacture and installation errors, and elastic cable deformation. One of the best ways to solve complex nonlinear error problems is using neural networks [27–29]. In order to fulfill the demands of various high-precision force sensing environments, such as surgical machines, Su *et al.* [30] introduced two multi-layer neural network approaches to enhance the sensing accuracy of the end-of-manipulator tool. Wang *et al.* [31] applied deep learning approach called uncertainty compensation model for the first time to aid robot dynamic parameter identification of six DOF robot manipulator for compensation of uncertain factors. Akhmetzyanov *et al.* [32] proposed the application of deep learning methods for kinematic error compensation of four-DOF cable-driven parallel robot. In addition, some scholars compensate and optimize the uncertainty factors of the robot through the method of online optimization estimation [33, 34]. Considering the complexity of the practical application of TSPS and the requirements of musculoskeletal robots, multi-layer neural networks are preferred to solve the problems of nonlinear friction, time-varying hysteresis, and elastic deformation of the cable. Moreover, this work also contains the following research:

1. The MAMS, which consists of the MC-AM and TSPS, is built with the benefits of distal mounting and mechanical traits resembling muscles. It may be utilized to build a multi-MAMS configuration musculoskeletal robot. We introduce the working concept, material choice, design strategy, and application examples.
2. The FF-MMN is proposed to solve the problems of nonlinear friction, time-varying hysteresis, and elastic deformation of the cable of TSPS. Moreover, the friction compensation performance trials of active and passive muscles are carried out using the simplest artificial muscle application

https://doi.org/10.1017/S026357472300005X Published online by Cambridge University Press

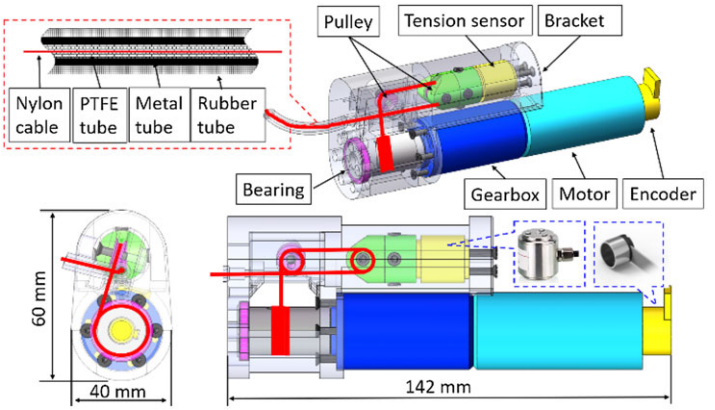

Figure 1. *Design schematic of MC-AM.*

system, and the relationship between the measurable input tension of TSPS and the unmeasurable output tension and cable elongation was discussed.

3. The application of LM-Arm, which includes seven DOF and 15 MAMSs is built in accordance with the anatomy of the arm. In addition, the experiments of end-point 3D trajectory tracking are conducted, and the result of trajectory error and muscle length error is discussed to verify the validity of the MAMS and LM-Arm.

The enhanced friction compensation technique of TSPS, the design of the MSMS, and FF-MMN method are presented in Section 2. The minimum artificial muscle application system and LM-Arm are built. Simultaneously, the verified experiments based on the minimum artificial muscle application system and LM-Arm are proposed in Section 3. The experimental findings and analyses are presented in Section 4. Section 5 finishes the project and suggests more work.

2. Material and method

Only tension can be produced by muscles. In this section, we propose a designed scheme of MSMS, including MC-AM and TSPS, and a method of the FF-MNN to compensate for friction of TSPS. Focuses on analyzing the existing tendon sheath–pulley mathematical models and discusses the relationship between the measurable input tension of TSPS and the unmeasurable output tension and cable elongation.

2.1. Design of MSMS

The skeleton is driven by a combination of active and passive muscles. The DC motor was selected as the power of MSMS in order to meet the requirements of high energy density, mature control, and remote installation. In order to tighten or loosen the cable, the winch is powered by the motor and reducer. Figure 1 shows the structural design of the MC-AM. The length, width, and height are 142 mm, 60 mm, and 40 mm, respectively. DC motors and reducers may be swapped out depending on the demands of various loads. The bracket is made from Nylon NO.7500 (HP3DHR-PA12) which is manufactured by high-precision 3D printing technology. The steel cable will be loose and broken due to wear under the condition of large curvature transmission, so we selected high-strength polyester fiber cable as the transmission medium [35]. The sheath is made up of a lubricated polytetrafluoroethylene (PTFE), a metal tube, and a rubber tube. The inner tube and cable are separated by a 0.2-mm gap, allowing the cable to slip freely within. To minimize friction between the cable and the supporting surface, the grease has been applied to the cable's surface.

https://doi.org/10.1017/S026357472300005X Published online by Cambridge University Press

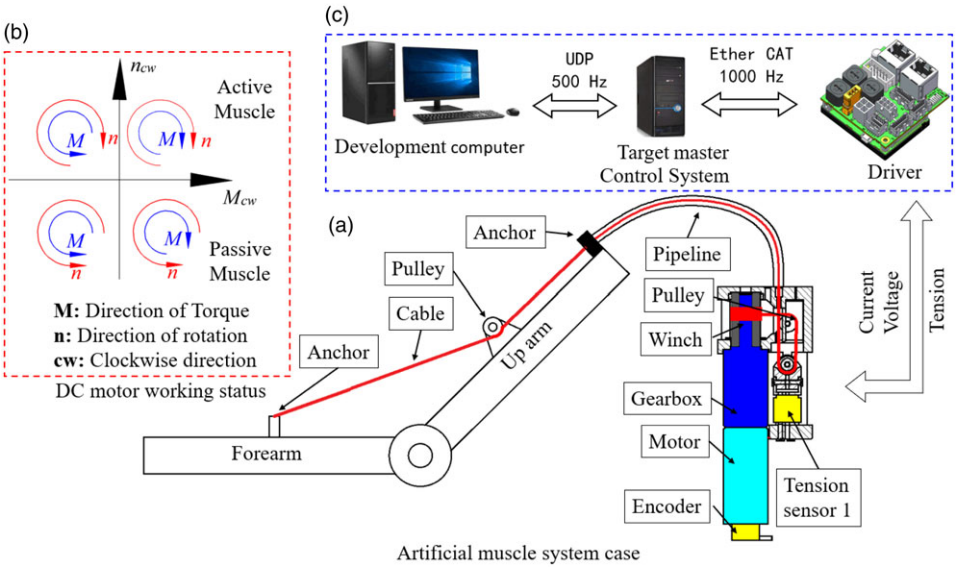

Figure 2. *Artificial muscle system case schematic.*

Figure 2(a) shows an application case of the MSMS. The TSPS can be used to transport that tension from MC-AM's output-end to the distal anchor. The benefit of this design is that the MC-AM is mounted at the remote of the load, reducing the weight of the equipment and increasing the number of configurable muscles on the skeleton. As shown in Fig. 2(b), the motor has four working modes. The active and passive working requirements of the muscles are represented by the first and fourth quadrants, respectively. The MSMS's circuit control scheme is depicted in Fig. 2(c). The industrial Ether CAT protocol is selected to connect the physical level (motors and various sensors) with the lower level (control system in Matlab/Simulink software) with a communication frequency of 1 kHz. The UDP protocol transmits data between lower level and higher level (development computer) with a communication frequency of 500 Hz. Such a control scheme can meet the information transmission in the case of multiple MSMS and multiple sensors, including muscle tension sensors, angle sensors, and vision sensors.

2.2. Friction compensation mathematical model of TSPS

The movement of the skeleton requires the antagonism of multiple MAMSs. TSPS can not only realize the transmission of muscle tension from the distal MC-AM to the skeleton anchor, but also brings negative problems such as nonlinear friction and elastic deformation of the cable. The tension equilibrium may be used to calculate the tension distribution along the cable at a quasi-static condition, producing the well-known Capstan equation [36].

$$dT = F = \mu N \cdot \delta; N = T(p)d\phi \tag{1}$$

$$T_{\text{out}} = T_{\text{in}} e^{-\mu\phi\cdot\delta} \tag{2}$$

where F is friction tension, $T(p)$ is the cable tension at position p along the cable, N is normal force exists between the cable and the inner wall of the sheath, and μ is a friction coefficient. δ is the sign of velocity of the cable relative to the sheath.

Due to factors such as the transmission efficiency of the cable itself, the lubricant viscosity, elastic cable deformation, the practical application of Eq. (2) to the cable drive is inapplicable. To accommodate the real operating circumstances, the friction model needs to be modified. A rudimentary musculoskeletal application scenario for one joint and two MAMSs is shown in Fig. 3. A tension sensor is installed at

https://doi.org/10.1017/S026357472300005X Published online by Cambridge University Press

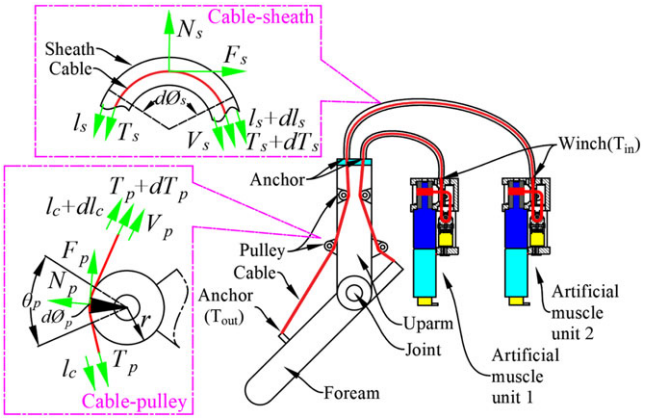

Figure 3. *Diagram of friction in the musculoskeletal system.*

the output end of the MC-AM, which is a closed-loop control between current and tension. The accuracy tension from MC-AM is assumed in this work. The combined transmission mode of TSPS is used from the MC-AM output end to the distal anchor of the skeleton. The joint angle affects the cable-pulley envelope angle. Considering the energy transfer efficiency of the cable itself, viscous friction, and reference [25, 26], we get

$$\phi = \sum_{i=1}^{n} \int_0^{\theta_{\mathrm{pi}}} d\phi_p + \int_0^{l_s} d\phi_s \tag{3}$$

$$v = \frac{dT_{\mathrm{in}}}{dt} \tag{4}$$

$$\mu = \delta(v) \tag{5}$$

$$\theta_{\mathrm{pi}} = H(q_i, r, n) \tag{6}$$

$$T_{\mathrm{out}} = \eta^{-\mathrm{sign}(v)} T_{\mathrm{in}} e^{-\mu\phi \cdot \mathrm{sign}(v)} + T_0 \tag{7}$$

where η is energy efficiency of the cable, ϕ is sum of cable bending angles; q is joint angle, ϕ_s and ϕ_p is elements of cable bending angle in cable sheath and cable pulley subsystem. Correspondingly, l_s is length of sheath, r is radius of pulley, n is number of pulley, θ_{pi} is pulley wrap angle relative to joint angle, $H(q_i, r, n)$ is the function of pulley wrap angle related to joint angle and number of pulley, T_{out} is tension of skeleton remote anchors, T_{in} is the tension at the output of the MC-AM, T_0 is pretension of the cable, and μ is viscosity coefficient function of relative velocity of cable relative to the sheath.

The feed-forward compensation rule follows the inverse of the Eq. (7):

$$T_r = \eta^{\mathrm{sign}(v_s)} T_s \left(1 - e^{\mu\phi \cdot \mathrm{sign}(v)}\right) \tag{8}$$

$$v_s = \frac{dT_j}{dt} \tag{9}$$

where, T_r is compensated friction. T_j is tension after filtering at the output of MA-AM (in order to prevent control jitter).

https://doi.org/10.1017/S026357472300005X Published online by Cambridge University Press

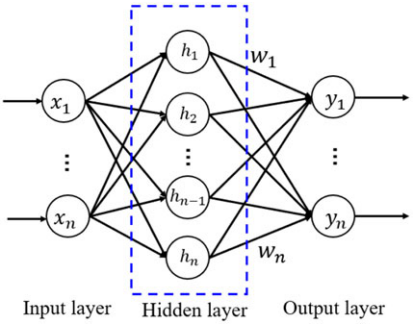

Figure 4. *Multilayer neural network structure diagram.*

2.3. Tendon elongation mathematical model of TSPS

The elastic deformation of cable would make the inaccurate position control of the system using TSPS. There is a serious problem for applications that require time-varying configurations of the TDPS but without equivalent sensory feedback at the distal end due to location limitations, such as surgical robots and musculoskeletal robot. As the main medium for transmitting tension, the cable will produce elastic deformation under the action of external tension. Incorporate references [21, 36], the elongation δ_l of the cable under input tension T_s as follows:

$$\delta_l = \begin{cases} \dfrac{\rho R}{\mu}\eta^{\text{sign}(v)}T_j\left(1 - e^{-\dfrac{\mu l}{R}\cdot\text{sign}(v)}\right) - \rho T_0 l_c & \text{if } l_c < L_1 \\ \dfrac{\rho R}{\mu}\eta^{\text{sign}(v)}T_j\left(1 - e^{-\dfrac{\mu L_1}{R}\cdot\text{sign}(v)}\right) - \rho T_0 L_1 & \text{if } l_c \geq L_1 \end{cases} \tag{10}$$

$$L_1 = \min\left\{l_c \in T_j\left(l_c\right) = T_0\right\} \tag{11}$$

where, l_c is length of cable. $\rho = \frac{1}{EA}$, E is the Youngs' modulus of cable, A is the cross-sectional area of the cable; R is the bending radius of the sheath; T_0 is pretension of the cable, L_1 is the maximum length along the tendon until where the input tension can be transmitted.

2.4. FF-MMN parameter identification method

The TSPS do not have standard consistency in design, manufacture, and installation, making friction compensation impossible through conventional model-based algorithms. As a flexible object, the cable will deform when it transmits the tension and generate nonlinear friction with the surface of the contacting object under the tension. It is difficult to complete the nonlinear regression prediction of friction by means of polynomial fitting. This section examines the relationship between the TSPS's measurable input tension and unmeasurable output tension as well as cable elongation using the FF-MMN, according to the theory depicted in Fig. 4. Although FF-MMN can establish complex functions and nonlinear relationships between a set of input and output data with multiple dimensions, there are still some limitations that need to be addressed, such as overfitting, underfitting, and serious time-consuming issues. In order to improve the prediction performance of the constructed model, such as high precision, stability and high velocity, this work adopts a FF-MNN method to establish the regression model of the TSPS. The principle formula is as follows:

https://doi.org/10.1017/S026357472300005X Published online by Cambridge University Press

$$y = W_0 \sum_{k=1}^{K} \Gamma \left(\sum_{i=1}^{N} \sum_{j=1}^{M} \left(W_{i,jk} \cdot X_{jk} + b_{jk} \right) \right) + b_0 \tag{12}$$

$$\Theta = \underset{\Theta}{\operatorname{argmin}} \sum_{t=1}^{N} \left(\hat{y}_t - y_t \right)^2 \tag{13}$$

where, X_{jk} is input of the jth neuron in the kth layer, $W_{i,jk}$ and b_{jk} are the weighting factors and bias, respectively. W_0 and b_0 are initial value of the weighting factors and bias, respectively. Θ is the optimal parameter, which can be calculated by the minimum least squares between the predicted result $\hat{y}$ and the real value y.

There are three common evaluation indices to measure the performance of the built FF-MNN models, namely mean square error (MSE), root mean square error (RMSE), and Pearson correlation coefficient ρ:

$$\mathrm{MSE} = \frac{\sum_{t=1}^{N} \left(\hat{y}_t - y_t \right)^2}{N} \tag{14}$$

$$\mathrm{RMSE} = \sqrt{\mathrm{MSE}} \tag{15}$$

$$\rho = \frac{1}{N-1} \sum_{t=1}^{N} \left(\frac{\hat{y}_t - \mu_{\hat{y}}}{\sigma_{\hat{y}}} \right) \left(\frac{y_t - \mu_y}{\sigma_y} \right) \tag{16}$$

where, the time t can be regarded as the number of observations. $\mu_{\hat{y}}$ and $\sigma_{\hat{y}}$ are the average and standard deviation of $\hat{y}$, while μ_y and σ_y are the same values of y. The best score for the Pearson correlation coefficient ρ is 1 while for the other errors, it is 0. The FF-MNN model aims to predict the tension close to the measured value.

Although there are alternative ways to evaluate sheath bending accumulation angle [37], they are not available in the musculoskeletal robot. In the musculoskeletal robot, the posture of the sheath and the number of pulleys are fixed, and the wrapping angle of the cable on the pulley is related to the joint angle q. According to Eqs. (8) and (10) we get

$$T_r = \tau(\Theta, T_s, l_s, v_c, q, n) \tag{17}$$

$$l_r = l(\Theta, T_s, v_c, q, l_c, L_1) \tag{18}$$

Where, q is the joint angle of the driven equipment, in order to calculate the wrap angle of the cable pulley.

The number of training samples and nodes is critical to the accuracy of the training results and the computation time. According to the experimental experience of TSPS, 500,000 (total time 500 s, sampling time 0.001 s) sample data and 30 nodes were selected for friction compensation and cable elongation rate prediction.

3. Experiment design

There are two sub-sections in this section. The first step in the process is to construct a minimal MSMS friction experiment bench to assess the performance of the TSPS. The other involves building an LM-Arm platform with seven DOF and 15 MSMSs then using end-point 3D trajectory tracking tests to verify the viability of MSMS and LM-Arm.

https://doi.org/10.1017/S026357472300005X Published online by Cambridge University Press

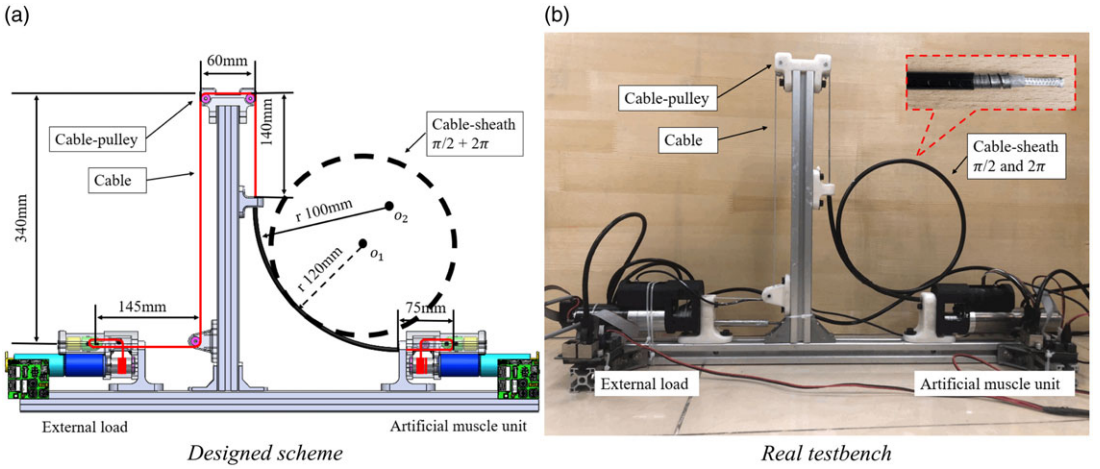

Figure 5. *Minimal MSMS friction experiment bench. (a) Designed scheme. (b) Real test bench.*

3.1. Experiment design of friction compensation

Figure 5 depicts the minimal MSMS friction experiment bench using two MA-AMs and a TSPS. One of MA-AM acts as the distal load and is coupled to the other end through TSPS. A transmission distance and the length of the sheath are around 1667 mm and 806 mm, correspondingly, which can accommodate most of the musculoskeletal system utilization requirements. Each MA-AM is equipped with a MAXON DC35 motor (rated power 120 W), an RV-type reducer (53:1), and a high-precision tension sensor. The 16 braided Nylon cable with a diameter of 3 mm is selected, and the Young's modulus of cable is about 1.4 GPa (the maximum allowable tension is about 800 N). The surface of the cable is coated with an appropriate amount of grease (MOLYKOTE G-0052FG, the viscosity is 115 cst at 40°C).

The tendon sheath friction related to the length and bending angle of the sheath have been studied by many scholars [26, 37, 38]. These principles are applicable to the time-varying sheath bending angle and feedback. The MSMS designed in this study is used under the condition that the sheath's length and posture remain unchanged. Under larger load and higher contraction velocity conditions, it is not possible to install additional sensors in the sheath. So that according to Eqs. (17) and (18), the experimental variables are designed as muscle tension (T_s and T_{out}) and muscle contraction velocity (v). The specific implementation method is as follows:

1. Experiments of active muscle: the motor working in the first quadrant supply a tension. The range of expected muscle tension (T_{out}) and contraction velocity (v) is 40–∼200 N and 0.02–∼0.12 m/s, respectively.
2. Experiments of passive muscle: the motor working in the fourth quadrant supply a tension. The range of expected muscle tension (T_{out}) and contraction velocity (v) is 40–∼200 N and −0.12–∼−0.02 m/s, respectively.

3.2. Design of LM-Arm

Based on the designed MSMS, we built the LM-Arm platform, which is strikingly comparable to the anatomy of the human arm [39]. As illustrated in Fig. 6, it consists of four skeleton (shoulder blade, humerus, ulna, and radius), seven DOF (shoulder three DOF, elbow one DOF, forearm one DOF, and wrist two DOF), and 15 MSMSs (the shoulder, elbow, forearm, and wrist joint have seven MSMSs, two MSMSs, two MSMSs, and four MSMSs, respectively). The lengths of upper arm, forearm, and hand are, respectively, 0.33 m, 0.39 m, and 0.26 m. It is essential to have a high-precision sensing system, which includes individual muscle tension and joint angle sensors. At least two MSMSs control each DOF, and

https://doi.org/10.1017/S026357472300005X Published online by Cambridge University Press

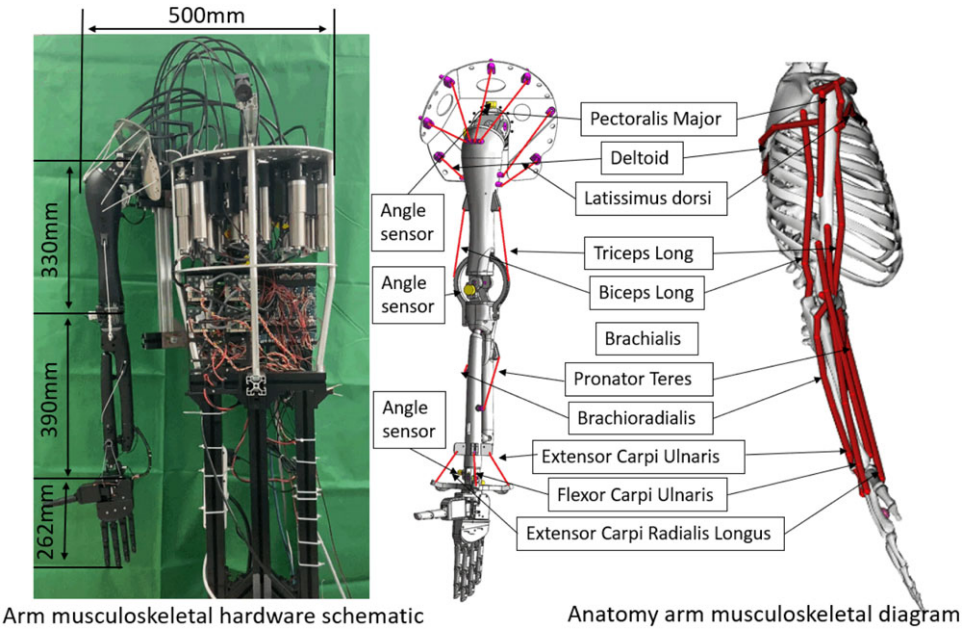

Figure 6. *LM-Arm design diagram.*

each MSMSs controls only one joint. This has the benefit of decreasing the coupling between the muscle and the joint space, provided that the antagonistic connection between the multiple muscles is satisfied.

Although friction compensation is carried out for MSMS, it cannot compensate for the manufacturing and installation errors and dynamic model errors. We therefore introduce a straightforward computational muscle force feedback control strategy to improve the effect of controlling LM-Arm. The control amount is accurate to the muscle tension. The kinematic of the skeletons refers to the method of *Denavit–Hartenberg* Matrix. We can calculate muscle length l according to the following formula.

$$l = g(q) \tag{19}$$

The Jacobian matrix $L(q)$ maps the relationship between muscle and joint space. Combined with the principle of virtual work [40], we get the following relation:

$$dl = -L(q)dq \tag{20}$$

$$\tau = -L(q) \cdot F \tag{21}$$

where, q is a vector of joint variables, muscle length matrix $dl = [dl_1, dl_2 \ldots dl_{15}]$; joint angle matrix $dq = [dq_1, dq_2 \ldots dq_7]$; $F = [f_1, f_2, f_3 \ldots f_{15}]$ is the muscle tension matrix; $\tau = [\tau_1, \tau_2, \tau_3 \ldots \tau_7]$ is joints torque matrix. The direction of muscular contraction is indicated by the negative sign. Optimize level of muscular tension under the following conditions:

$$\min_{F_d} \|F_d\|^2 \text{ Subject to } \begin{cases} \tau = -L(q) \cdot F_d \\ F_{\min} \le F_d \le F_{\max} \end{cases} \tag{22}$$

where, F_d is optimal muscle tension; $F_{\min}$ and $F_{\max}$ is upper and lower limits of muscle tension.

The dynamic of LM-Arm is calculated with *Lagrangian* dynamic:

$$H[-\dot{L}^{+}(q)\dot{l} - L(q)\ddot{l}] - \Theta \mathrm{L}^{+}(q)\dot{l} + G = -L(q)F - d \tag{23}$$

https://doi.org/10.1017/S026357472300005X Published online by Cambridge University Press

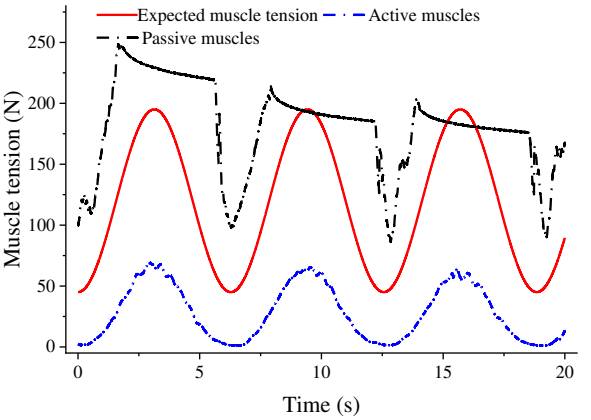

Figure 7. *Experimental results no friction compensation .*

where H represents a symmetric positive defined inertia matrix, Θ denotes the Centripetal and Coriolis force, G is the gravitational force, F is muscle tension, and d represents the uncertain interference of system friction and model error.

We estimated the compensated muscle acceleration through the error of muscle length and muscle velocity. The formula is as follows:

$$\Delta l = l_e - l \tag{24}$$

$$\Delta \dot{l} = \dot{l}_e - \dot{l} \tag{25}$$

$$\Delta \ddot{l} = A \cdot \Delta l - B \cdot \Delta \dot{l} \tag{26}$$

where l_e is the desired muscle length; l is the measured muscle length; $\dot{l}_e$ is the desired muscle velocity; $\dot{l}$ is the measured muscle velocity; Δl, $\Delta \dot{l}$ are error of muscle length, muscle velocity, respectively. $\Delta \ddot{l}$ is the compensation of muscle acceleration; A and B are proportional coefficient and differential coefficient, correspondingly.

To test the flexibility of LM-Arm and the performance of MSMS, we build a sin-function end-point 3D trajectory tracking with two period and an amplitude of 0.15 m. We adjusted the running time to 115 s and repeat the experiment six times.

4. Results and discussion

The experimental findings of friction compensation and LM-Arm end-point 3D trajectory tracking are examined in this section. Analysis of muscle tension and elongation in active and passive modes is done to account for friction compensation. The experiments' analytical criteria for trajectory tracking include tracking error and muscle length error. The performance of the MSMS and the effect of the LM-Arm is confirmed by experiments.

4.1. Experiment results of friction compensation

The experiments of the performance of MSMS were carried out using the apparatus described in Section 3.1. The findings of the active and passive muscles are shown in Fig. 7 before friction compensation, and it is evident that there is a significant average inaccuracy of 88.5 N and 63.9 N, respectively. An error of this magnitude cannot be utilized routinely. Figure 8 displays the results of active and passive muscles following FF-MNN. The outcomes demonstrated that both active and passive muscle tension measured

https://doi.org/10.1017/S026357472300005X Published online by Cambridge University Press

Table I. *Experimental results of FF-MNN friction compensation.*

		Muscle contraction velocity (m/s)						
Object	**Index**	**0.02**	**0.04**	**0.06**	**0.08**	**0.1**	**0.12**	**Average value**
Active muscle	MSE (N)	3.72	1.56	1.43	3.02	3.98	4.38	3.02
	RMSE (N)	1.92	1.25	1.20	1.74	1.99	2.09	1.70
	ρ	0.9953	0.9996	0.9992	0.9966	0.9941	0.9938	0.9964
Passive muscle	MSE (N)	1.27	1.02	1.89	1.60	1.75	1.66	1.53
	RMSE (N)	1.13	1.01	1.37	1.26	1.32	1.29	1.23
	ρ	0.9992	0.9997	0.9993	0.9995	0.9994	0.9990	0.9994

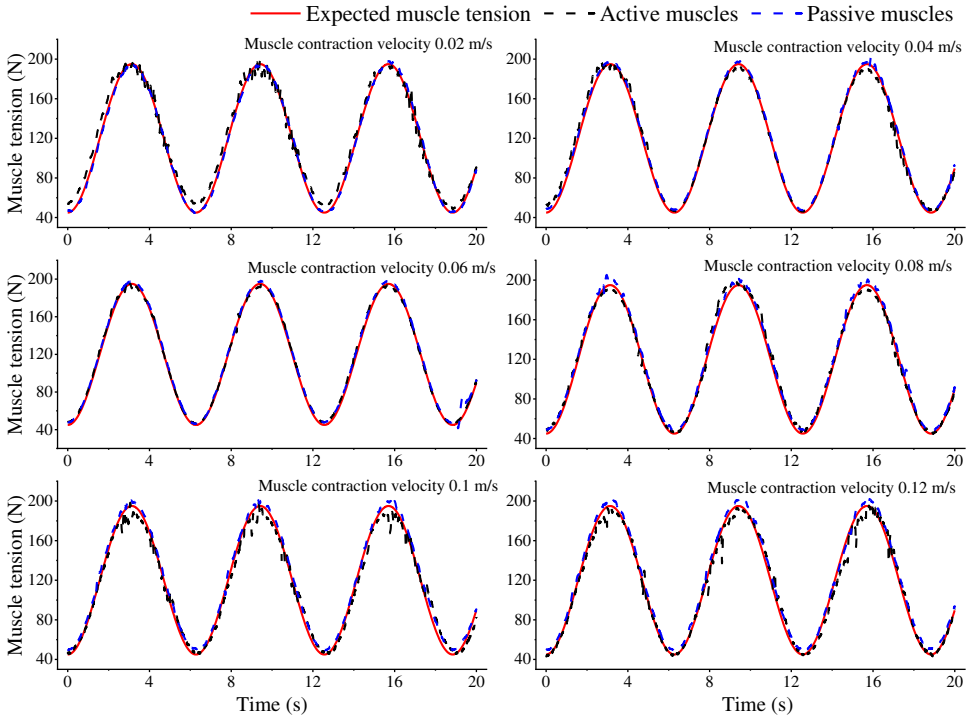

Figure 8. *Experimental results of FF-MNN friction compensation.*

at the load were consistent with the expected value. The total performance of active muscles is inferior to that of passive muscles, according to the assessment indications. When the expected muscle tension is stronger, the error is larger (e.g. the crest part). The actual muscle tension curve is rather smooth when the muscle contraction velocity is between 0.04 m/s and 0.06 m/s, but the jitter increases at high contraction velocity, especially when the muscle contraction velocity is over 0.08 m/s. Others results are shown in Table I, and every indicator shows that performance of passive muscle is superior to active muscle. The best results of MSE, RMSE, and ρ-value are 1.08 N, 1.04 N and 0.9998, respectively. When the passive muscle contraction velocity is 0.04 m/s. The worst results are the active muscle contraction velocity of 0.1 m/s and 0.12 m/s. The MES and RMSE were higher than 6.5 N and 2.5 N, respectively, and the ρ-value was as low as 0.994.

The cable can only produce a unidirectional tension. When a larger tension needs to be provided, the deformation of the cable increases, so that the inner elastic tension increases. As a result, the nonlinear interference of the system is enhanced, resulting in the situation of curve jitter and large error. The

https://doi.org/10.1017/S026357472300005X Published online by Cambridge University Press

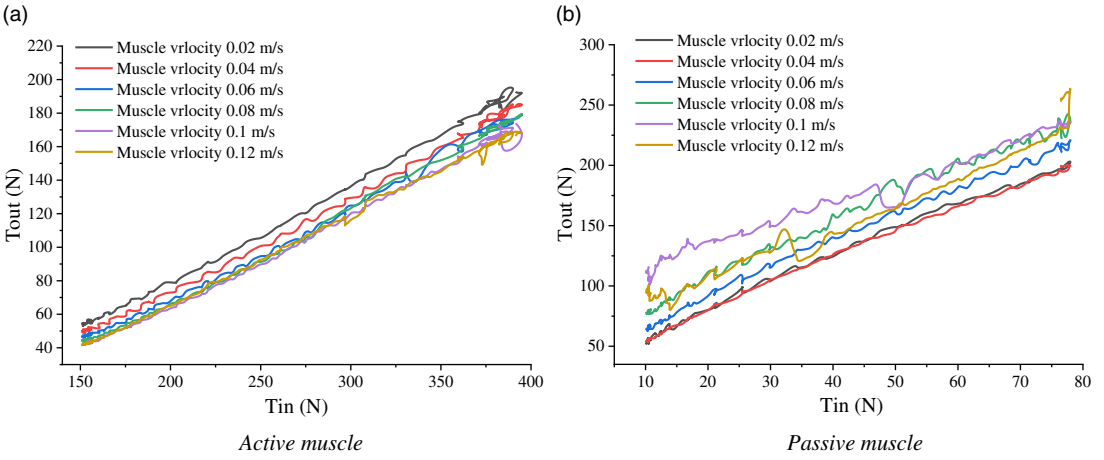

Figure 9. *Input force and output muscle tension results. (a) Active muscle. (b) Passive muscle.*

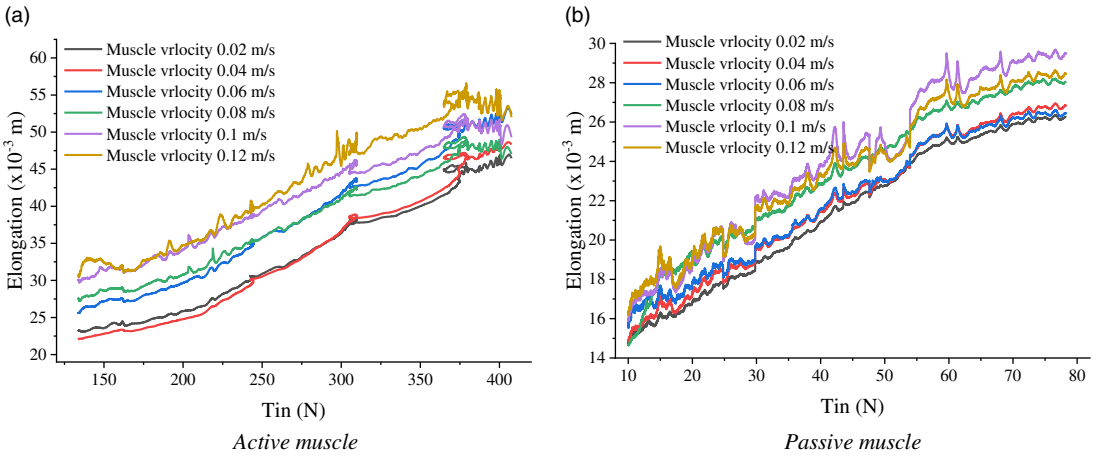

Figure 10. *Relationship between input muscle tension and cable deformation. (a) Active muscle. (b) Passive muscle.*

tension sensors are installed on both the MC-AM and the load end of the experimental bench system, and the experiment's objective is to make the load end tension compatible with the expected value. When a MSMS is utilized passively, the frictional tension acts as a part of the expected tension, so that the intrinsic tension of cable is small. So that the actual muscle tension curve smooth, which is consistent with the results in Fig. 10. In general, the average errors of active and passive muscles are 3.87 N (standard deviation 3.02 N) and 3.51 N (standard deviation 1.53 N), respectively. This outcome complies with the criteria for using MSMS in the musculoskeletal robot.

The relationship between the input muscle tension and the output muscle tension of TSPS is analyzed more deeply under different muscle contraction velocity conditions, as shown in Fig. 9. The input and output muscle tension is close to a linear relationship. The contraction velocity has little impact on the active muscle. On the contrary, it has a greater impact on the passive muscle. In addition, when contraction velocity increases, fluctuations become more noticeable. When the input force is large, there is a larger jitter in the active muscle, which is compatible with the Fig. 8. Table II displays the mean energy efficiency and standard deviation data for active and passive muscles at various velocities. Taken together, the average efficiency of the active and passive muscles is 0.408 (standard deviation 0.062) and 4.36 (standard deviation 1.55), respectively. Although the TSPS has significantly poorer energy

https://doi.org/10.1017/S026357472300005X Published online by Cambridge University Press

Table II. *Energy efficiency results.*

		Muscle contraction velocity (m/s)						
Object	**Index**	**0.02**	**0.04**	**0.06**	**0.08**	**0.1**	**0.12**	**Average value**
Active muscle	Average efficiency	0.436	0.406	0.404	0.417	0.387	0.396	0.408
	Standard deviation	0.048	0.062	0.063	0.078	0.061	0.061	0.062
Passive muscle	Average efficiency	3.594	3.564	4.033	4.62	5.607	4.743	4.36
	Standard deviation	0.94	0.943	1.194	1.549	2.676	2.019	1.55

Table III. *Cable elongation results.*

		Muscle contraction velocity (m/s)						
Object	**Index**	**0.02**	**0.04**	**0.06**	**0.08**	**0.1**	**0.12**	**Average value**
Active muscle	Average efficiency ($\times 10^{-3}$ m/N/m)	0.125	0.125	0.142	0.141	0.153	0.16	0.141
	Standard deviation ($\times 10^{-3}$ m/N/m)	0.0123	0.0097	0.0139	0.0195	0.023	0.0219	0.0167
Passive muscle	Average efficiency ($\times 10^{-3}$ m/N/m)	0.58	0.55	0.583	0.678	0.66	0.643	0.615
	Standard deviation ($\times 10^{-3}$ m/N/m)	0.239	0.224	0.299	0.286	0.266	0.323	0.273

transfer efficiency than gears, belts, and connecting rods, its advantages, such as distant transmission and adaptability to challenging and constrained paths, are incomparable. The transmission efficiencies of active and passive muscles can complement each other to achieve an acceptable overall efficiency. An ideal use effect can still be obtained through an FF-MNN method.

To achieve accurate position control, it is necessary to study cable elongation for the TSPS. The cable elongation has an approximate linear relationship with the input muscle tension, but when the input muscle tension or contraction velocity is large, there is a significant jitter, as shown in Fig. 10. The mean elongations of active and passive muscle is 0.141 mm/N/m (standard deviation 0.017 mm/N/m) and 0.615 mm/N/m (standard deviation 0.273 mm/N/m), respectively. Others results are shown in Table III. The inaccurate position control of MSMS is more likely to occur when the muscle tension and contraction velocity are large. The cable elongation is essential for the TSPS to provide precise position control. The findings of this experiment demonstrate that the input muscle tension and cable elongation have a clear relationship that may be utilized to increase the control precision of practical robots such as surgical robots, dexterous hands, and rescue robots, among others.

4.2.3 D trajectory tracking experimental results of LM-Arm

The primary purpose of the MSMS is to construct a musculoskeletal robot, so that we can evaluate the end-point trajectory tracking of the LM-Arm to determine the effective performance of MSMS. The experimental bench and scheme are described in Section 3.2. According to the findings, shown in Fig. 11, the six experiments' end-point trajectories are consistent with the expected trajectories, with a maximum trajectories error of approximately 0.039 m (3.9%). The sin-function trajectory near starting point has the highest error, which is brought on by an unbalanced trajectory at the transition location. The mean of the trajectory of the six experiments is 0.0158 m (1.6%), and the standard deviation is 0.0071 m. The trajectory error can comprehensively show the performance of the tension control of MSMS, and it is feasible to construct the complex musculoskeletal robot by designing the MSMS.

https://doi.org/10.1017/S026357472300005X Published online by Cambridge University Press

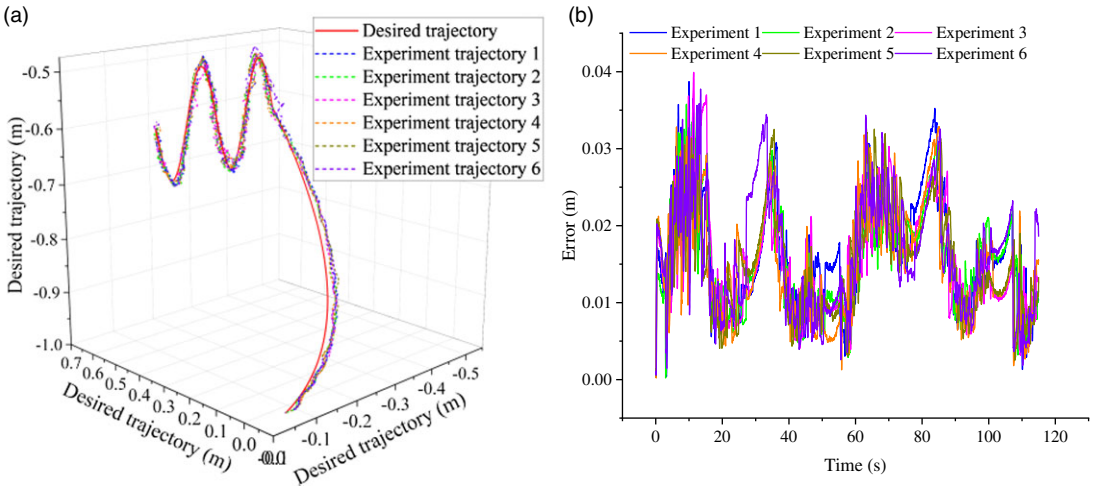

Figure 11. *Trajectory tracking results of LM-Arm. (a) Trajectory results. (b) Trajectory error results.*

To gain a deeper understanding of the controllable performance of the MSMS, we selected the muscle length data from one set of experiments for analysis, as shown in Fig. 12. The results show that the actual feedback length of the 15 MSMS is basically the same as the expected value, but it can be seen from the curve that the error of the last six MSMS is larger. There are two reasons for this result: the first is that the MSMS (#10–#15) provide tension for the forearm and wrist joint. Moreover, the longer transmission distance the weaker friction compensation effect. The second reason is that the forearm and wrist joints provide dexterity functions, and the greater muscle contraction velocity leads to friction-compensated jitter, which is consistent with the results in Figs. 8–10. As shown in Fig. 13, the mean error and standard deviation in muscle length are 0.00078 m (0.72%) and 0.0004 m, respectively. According to the findings, the MSMS's control performance is comparatively steady, and the proposed FF-MNN friction compensation method has produced positive outcomes. Despite the use of feedback control in this experiment, based on the experimental results of muscle length error, the designed MSMS will be able to drive the musculoskeletal robot to perform daily tasks.

5. Conclusion

The MSMS, including MC-AM and TSPS, is designed in this study. The strong nonlinear friction problem of the TSPS is solved using the FF-MNN approach. The MSMS has three advantages: (1) To measure output tension or position, it does not require sensors to be attached to the cable's output port or other, which enables the use of musculoskeletal robot with restricted sensor applications and reduces the size and complexity of the end-effector; (2) MC-AM has the advantages of small size, high energy density, and mature control technology and can easily install multiple sets in a small space. For example, LM-Arm can install 15 MC-AMs in the chest cavity; (3) MSMS can simulate the active and passive working state of muscles under larger load and higher velocity conditions to meet the motion requirements of skeleton; (4) The proposed MSMS is low cost, adding only a few dollars to the whole system. This is very inexpensive compared to the cost of the other system, for example PAM. The experiments using the smallest artificial muscle system demonstrate that the average errors of actual active and passive muscle tension compared to expected value are 3.87 N and 3.51 N, respectively, under conditions of larger load and higher contraction velocity. Based on this, we built an LM-Arm with seven DOF and 15 MSMSs. 3D trajectory tracking investigations confirm the LM-Arm's effectiveness. The average error of the end-point trajectory and muscle length is 0.0158 m (1.6%) and 0.00078 m (0.72%), respectively.

https://doi.org/10.1017/S026357472300005X Published online by Cambridge University Press

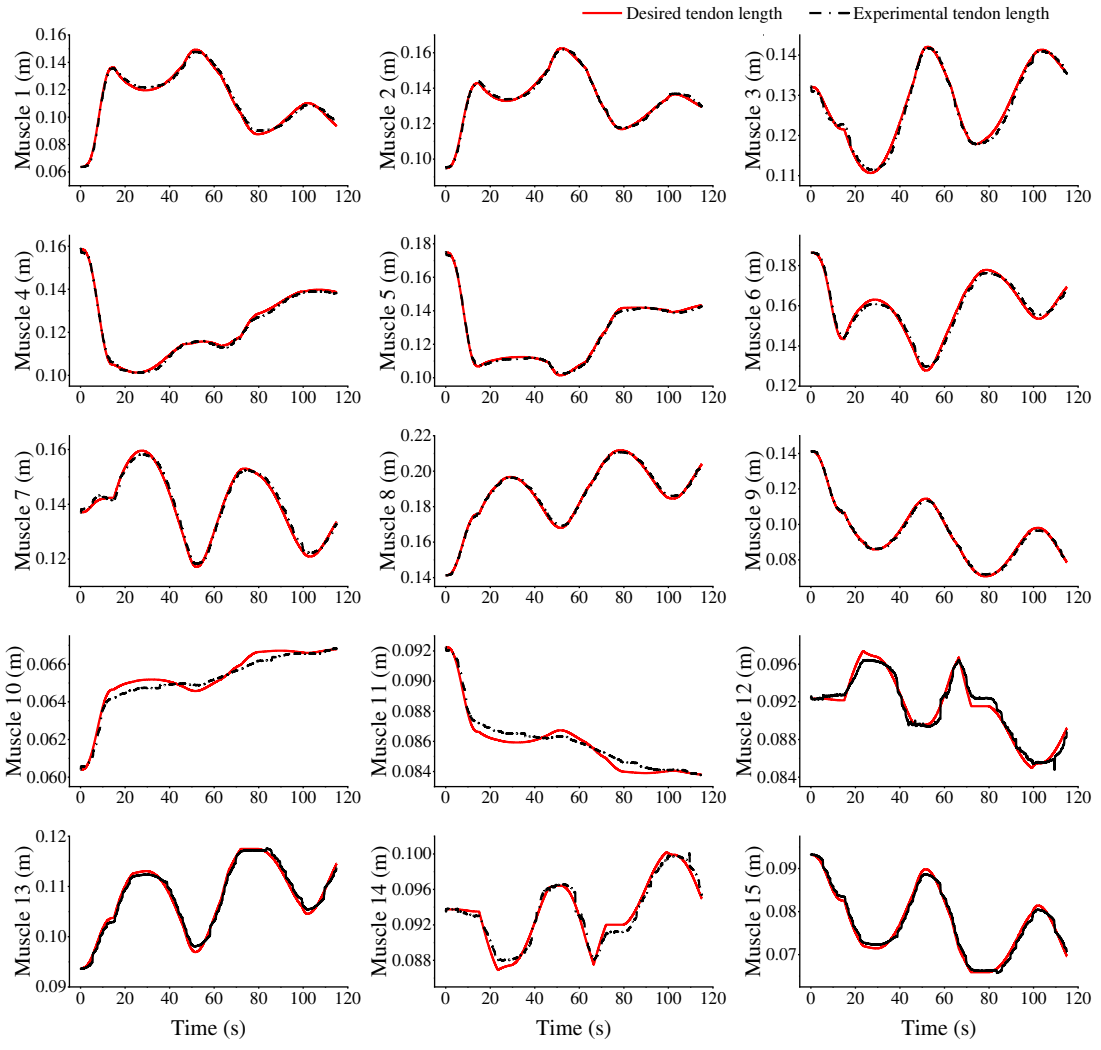

Figure 12. *Muscle length results of LM-Arm.*

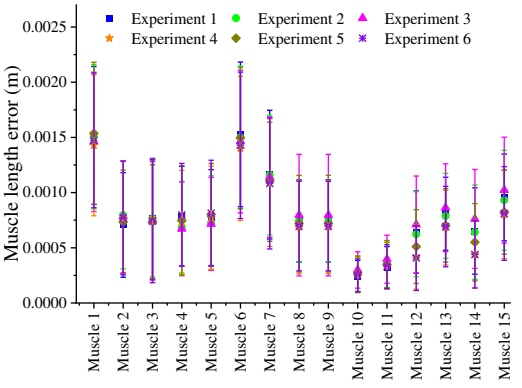

Figure 13. *Statistical muscle length error results of LM-Arm.*

https://doi.org/10.1017/S026357472300005X Published online by Cambridge University Press

The proposed model requires no sensory feedback from the distal end, but still can provide commensurable estimation accuracy by monitoring the consequential changes in the configuration after the initial calibration. MSMS can not only build complex musculoskeletal robots, but also can be used for devices with strict requirements on power source and tension transmission path, such as rescue robots, wearable flexible robots, and abdominal invasive surgical robots.

Although some of the issues with TSPS are addressed by this work, there are still several restrictions on its application, such as its low efficiency and propensity for cable breakage. In the future work, we will focus on more wear-resistant and high-strength cable and sheath structure with smaller friction coefficients to improve the performance of MSMS from the mechanical and material aspects. In the application of MSMS, in addition to building LM-Arm, the design of muscular dexterous hands is also one of the key directions.

Author contributions. Jianbo Yuan performed mathematical formula conception, experimental design, experimental implementation, experimental data processing, and paper writing.

Yerui Fan performed experimental implementation.

Yaxiong Wu performed experimental design and experimental implementation.

Financial support. This work is supported partly by the National Key Research and Development Program of China (2017YFB1300203), partly by the National Natural Science Foundation of China (NSFC) (under Grants 61627808, 91648205), partly by the Strategic Priority Research Program of Chinese Academy of Science under Grant XDB32000000.

Conflicts of interest. No conflict of interest exists in the submission of this manuscript, and manuscript is approved by all authors for publication. I would like to declare on behalf of my coauthors that the work described was original research that has not been published previously, and not under consideration for publication elsewhere, in whole or in part.

Ethical approval. Not applicable.

References

[1] K. R. S. Holzbaur, W. M. Murray and S. L. Delp, "A model of the upper extremity for simulating musculoskeletal surgery and analyzing neuromuscular control," *Ann. Biomed. Eng.* **33**(6), 829–840 (2005).

[2] N. Margareta and H. F.Victor. *Basic Biomechanics of the Musculoskeletal System* (Julie K. Stegman, Philadelphia, 2012).

[3] X. Huang, W. Wu and H. Qiao, "Connecting model-based and model-free control with emotion modulation in learning systems," *IEEE Trans. Syst. Man Cybern. Syst.* **51**(8), 4624–4638 (2021).

[4] X. Huang, W. Wu, H. Qiao and Y. Ji, "Brain-inspired motion learning in recurrent neural network with emotion modulation," *IEEE Trans. Cogn. Dev. Syst.* **10**(4), 1153–1164 (2018).

[5] H. Qiao, J. Chen and X. Huang, "A survey of brain-inspired intelligent robots: Integration of vision, decision, motion control, and musculoskeletal systems," *IEEE Trans. Cybern.* **52**(10), 11267–11280 (2021).

[6] S. Kurumaya, H. Nabae, G. Endo and K. Suzumori, "Design of thin McKibben muscle and multifilament structure," *Sens. Actuators A Phys.* **261**, 66–74 (2017).

[7] S. Tawfick and Y. Tang, "Stronger artificial muscles, with a twist," *Science (New York, N.Y.)* **365**(6449), 125–126 (2019).

[8] S. Li, D. M. Vogt, D. Rus and R. J. Wood, "Fluid-driven origami-inspired artificial muscles," *Proc. Natl. Acad. Sci.* **114**(50), 13132–13137 (2017).

[9] K. H. Cho, Y. Kim, S. Y. Yang, K. Kim, J. H. Park, H. Rodrigue, H. Moon, J. C. Koo, J. Nam and H. R. Choi, "Artificial musculoskeletal actuation module driven by twisted and coiled soft actuators," *Smart Mater. Struct.* **28**(12), 125010 (2019).

[10] E. Acome, S. K. Mitchell, T. G. Morrissey, M. B. Emmett, C. Benjamin, M. King, M. Radakovitz and C. Keplinger, "Hydraulically amplified self-healing electrostatic actuators with muscle-like performance," *Science* **359**(6371), 61–65 (2018).

[11] Y. Asano, K. Okada and M. Inaba, "Design principles of a human mimetic humanoid: Humanoid platform to study human intelligence and internal body system," *Sci. Robot.* **2**(13), eaaq0899 (2017).

[12] A. Hitzmann, H. Masuda, S. Ikemoto and K. Hosoda, "Anthropomorphic musculoskeletal 10 degrees-of-freedom robot arm driven by pneumatic artificial muscles," *Adv. Robot.* **32**(15), 865–878 (2018).

[13] M. Kanik, S. Orguc, G. Varnavides, J. Kim, T. Benavides, D. Gonzalez, T. Akintilo, C. C. Tasan, A. P. Chandrakasan, Y. Fink and P. Anikeeva, "Strain-programmable fiber-based artificial muscle," *Science (American Association for the Advancement of Science)* **365**(6449), 145–150 (2019).

[14] J. Yuan, Y. Wu, B. Wang and H. Qiao, "Musculoskeletal Robot with Motor Driven Artificial Muscle," **In:** *2021 6th IEEE International Conference on Advanced Robotics and Mechatronics* (2021).

https://doi.org/10.1017/S026357472300005X Published online by Cambridge University Press

[15] S. Min and S. Yi, "Development of cable-driven anthropomorphic robot hand∗," *IEEE Robot. Autom. Lett.* **6**(2), 1176–1183 (2021).
[16] M. Dežman, T. Asfour, A. Ude and A. Gams, "Mechanical design and friction modelling of a cable-driven upper-limb exoskeleton," *Mech. Mach. Theory* **171**(1), 104746 (2022).
[17] E. Idà, S. Briot and M. Carricato, "Identification of the inertial parameters of underactuated cable-driven parallel robots," *Mech. Mach. Theory* **167**(6), 104504 (2022).
[18] K. Watanabe, T. Kanno, K. Ito and K. Kawashima, "Single-master dual-slave surgical robot with automated relay of suture needle," *IEEE Trans. Ind. Electron.* **65**(8), 6343–6351 (2018).
[19] Y. Ding, M. Kim, S. Kuindersma and C. J. Walsh, "Human-in-the-loop optimization of hip assistance with a soft exosuit during walking," *Sci. Robot.* **3**(15), eaar5438 (2018).
[20] C. J. Nycz, T. Butzer, O. Lambercy, J. Arata, G. S. Fischer and R. Gassert, "Design and characterization of a lightweight and fully portable remote actuation system for use with a hand exoskeleton," *IEEE Robot. Autom. Lett.* **1**(2), 976–983 (2016).
[21] Z. Wang, Z. Sun and S. J. Phee, "Modeling tendon-sheath mechanism with flexible configurations for robot control," *Robotica* **31**(7), 1131–1142 (2013).
[22] Z. Sun, Z. Wang and S. J. Phee, "Elongation modeling and compensation for the flexible tendon–sheath system," *IEEE/ASME Trans. Mechatron.* **19**(4), 1243–1250 (2014).
[23] T. N. Do, T. Tjahjowidodo, M. W. S. Lau and S. J. Phee, "An investigation of friction-based tendon sheath model appropriate for control purposes," *Mech. Syst. Signal Process.* **42**(1-2), 97–114 (2014).
[24] Q. Wu, X. Wang, L. Chen and F. Du, "Transmission model and compensation control of double-tendon-sheath actuation system," *IEEE Trans. Ind. Electron.* **62**(3), 1599–1609 (2015).
[25] H. Wang, J. Kinugawa and K. Kosuge, "Exact kinematic modeling and identification of reconfigurable cable-driven robots with dual-pulley cable guiding mechanisms," *IEEE/ASME Trans. Mechatron.* **24**(2), 774–784 (2019).
[26] U. Jeong and K. Cho, "Control of a bowden-cable actuation system with embedded BoASensor for soft wearable robots," *IEEE Trans. Ind. Electron.* **67**(9), 7669–7680 (2020).
[27] S. Wang, J. Na and Y. Xing, "Adaptive optimal parameter estimation and control of servo mechanisms: Theory and experiments," *IEEE Trans. Ind. Electron.* **68**(1), 598–608 (2021).
[28] J. Na, Y. Xing and R. Costa-Castello, "Adaptive estimation of time-varying parameters with application to roto-magnet plant," *IEEE Trans. Syst. Man Cybern. Syst.* **51**(2), 731–741 (2021).
[29] C. Yang, Y. Jiang, W. He, J. Na, Z. Li and B. Xu, "Adaptive parameter estimation and control design for robot manipulators with finite-time convergence," *IEEE Trans. Ind. Electron.* **65**(10), 8112–8123 (2018).
[30] H. Su, W. Qi, Y. Hu, J. Sandoval, L. Zhang, Y. Schmirander, G. Chen, A. Aliverti, A. Knoll, G. Ferrigno and E. De Momi, "Towards model-free tool dynamic identification and calibration using multi-layer neural network," *Sensors (Basel)* **19**(17), 3636 (2019).
[31] S. Wang, X. Shao, L. Yang and N. Liu, "Deep learning aided dynamic parameter identification of 6-DOF robot manipulators," *IEEE Access* **8**, 138102–138116 (2020).
[32] A. Akhmetzyanov, M. Rassabin, A. Maloletov, M. Fadeev and A. Klimchik, "Deep Learning with Transfer Learning Method for Error Compensation of Cable-driven Robot," **In:** *17th International Conference on Informatics in Control, Automation and Robotics* (2020).
[33] J. Lu, F. Richter and M. Yip, "Pose estimation for robot manipulators via keypoint optimization and sim-to-real transfer," *IEEE Robot. Autom. Lett.* **7**(2), 4622–4629 (2021).
[34] P. Salaris, M. Cognetti, R. Spica and P. R. Giordano, "Online optimal perception-aware trajectory generation," *IEEE Trans. Robot.* **35**(6), 1307–1322 (2019).
[35] X. G. Cui, J. Geng and J. W. Ding, "Study on experiment of terminal fixture connection of steel wire rope," *Appl. Mech. Mater.* **351-352**, 1415–1418 (2013).
[36] M. Kaneko, T. Yamashita and K. Tanie, "Basic Considerations on Transmission Characteristics for Tendon Drive Robots," **In:** *Fifth International Conference on Advanced Robotics 'Robots in Unstructured Environments'*, vol. **1** (1991) pp. 827–832.
[37] U. Jeong and K. Cho, "A novel low-cost, large curvature bend sensor based on a bowden-cable," *Sensors* **16**(7), 961 (2016).
[38] Y. Liang, Z. Du, W. Wang and L. Sun, "A novel position compensation scheme for cable-pulley mechanisms used in laparoscopic surgical robots," *Sensors* **17**(10), 2257 (2017).
[39] S. Zhong, J. Chen, X. Niu, H. Fu and H. Qiao, "Reducing redundancy of musculoskeletal robot with convex hull vertexes selection," *IEEE Trans. Cogn. Dev. Syst.* **12**(3), 601–617 (2020).
[40] V. De Sapio, J. Warren, O. Khatib and S. Delp, "Simulating the task-level control of human motion: A methodology and framework for implementation," *Vis. Comput.* **21**(5), 289–302 (2005).

Cite this article: J. Yuan, Y. Fan and Y. Wu (2023). "Design of motor cable artificial muscle (MC-AM) with tendon sheath–pulley system (TSPS) for musculoskeletal robot", Robotica **41**, 1634–1650. https://doi.org/10.1017/S026357472300005X